JOURNAL OF SPACECRAFT AND ROCKETS
Vol. 32, No. 3, May–June 1995

Suborbital Launch Trajectories for Satellite Delivery

Mark R. Goodell*
Patrick Air Force Base, Florida 32925-3299
and
William C. Elrod†
U.S. Air Force Institute of Technology, Wright Patterson Air Force Base, Ohio 45433-7765

The utility of suborbital launch trajectories to increase the payload capacity for a hypersonic-lifting-body launch vehicle was investigated. This type of trajectory involves deployment of a payload and booster motor from the launch vehicle at suborbital speed. A payload booster motor is required to insert the spacecraft into orbit while the launch vehicle re-enters and returns to earth. For this study, a simplified analytical technique was developed to estimate the payload capacity (not including booster motor) of various suborbital launch trajectories. Comparison with a detailed trajectory simulation showed that the simplified technique provided a reasonable estimate of suborbital trajectory performance. Results indicated that depending on certain vehicle and flight parameters, a hypersonic lifting body following a suborbital ascent trajectory could increase the payload-to-orbit weight by up to 61%.

Nomenclature

G	= universal gravitational constant, 6.67×10^{-11} N m^2/kg^2
g_0	= sea-level gravitational acceleration, m/s
H	= altitude from earth surface to point along flight path, m
h	= nondimensional altitude, H/H_{orbit}
I_{sp}	= propellant or fuel specific impulse, F/w, s
$I_{\text{sp eff}}$	= effective airbreathing specific impulse, s
M	= mass of the earth, 5.975×10^{24} kg
$\dot{m}$	= propellant mass flow rate
m_l, m_p, m_s	= launch-vehicle payload, propellant, and structure mass, kg
$m_{l\,\text{so}}, m_{l\,\text{so}}$	= booster–kickmotor payload and initial weight for suborbital trajectories, kg
m_0, m_f	= launch-vehicle initial and final mass (also used to represent initial and final mass for a given ascent trajectory segment), kg
q	= dynamic pressure, Pa
R, R_1, R_2, R_3	= initial-to-final vehicle mass ratios for trajectory segments, m_0/m_f
R_{so}	= initial-to-final mass ratio of segment 3 for suborbital trajectory
r, r_i, r_f	= altitude measured from center of earth to trajectory location, m
r_{cir}	= altitude of circular orbit from center of earth, m
V, V_i, V_f	= velocity at different trajectory locations, m/s
V_{cir}	= orbital velocity of circular target orbit, m/s
Z	= atmospheric scale height, 6982 m
μ	= gravitational parameter, GM, 3.99×10^{14} N m^2/kg
ξ	= orbit specific mechanical energy, m^2/s^2
Π_l, Π_p, Π_s	= launch vehicle payload, propellant and structural mass fraction
ρ, ρ_0	= air density at point along trajectory, and at sea level, kg/m^3

Subscripts

1, 2, 3	= trajectory segments
i, f	= initial and final conditions for a segment

Received Oct. 29, 1993; revision received Dec. 16, 1994; accepted for publication Dec. 16, 1994.

*Air Force Launch Controller, 45 Operations Group, 1201 Minuteman Street.

†Professor Emeritus, 2950 P Street. Associate Fellow AIAA.

Introduction

THE gravity-gradient launch trajectory has become widely accepted for space launches using today's multistage rocket vehicles. This is due primarily to structural and aerodynamic characteristics that are inherent in current multistage designs. A gravity-gradient trajectory flies at near-0-deg angle of attack during the launch ascent and thus produces minimum vehicle bending stress. By not taking advantage of atmospheric lifting forces, the gravity-gradient trajectory is not an efficient one with regard to energy requirements. Recent approaches for launch vehicle design represent a tendency towards the use of more efficient and flexible launch trajectories in the future. Specifically, future launch platforms may incorporate lifting surfaces and air-breathing propulsion technology that will provide improved maneuverability and fuel efficiency. Given the required technological advancements, a single-stage-to-orbit (SSTO) vehicle with these features may be practical.

The flight characteristics of a hypersonic-lifting-body vehicle would allow a variety of different ascent trajectories to be used, based on the mission and size of payload to be delivered into orbit. This paper presents the results of an analysis of hypersonic launch vehicle suborbital trajectories where only the payload is placed in orbit. Suborbital trajectory results are compared with the payload delivery capability of a baseline trajectory where both the hypersonic launch vehicle and the payload are placed in orbit.

One of the primary accomplishments of this study was the development of a simplified energy analysis method to facilitate the process required for the analysis of suborbital trajectories. While use of the energy analysis method required some specific information concerning launch-vehicle design and ascent profile, once this information was obtained, the calculations required for a first-order design estimate were greatly simplified. The energy analysis method involved calculation of baseline performance parameters using a standard ascent trajectory where both the payload and the launch vehicle were placed in the target orbit. Performance parameters were then determined for the same vehicle flying a suborbital ascent trajectory where the launch vehicle does not achieve orbital velocity and the payload is placed in orbit by means of an additional booster rocket motor. Data from this analysis were compared with similar calculations from a commercially available trajectory optimization computer program, with good agreement.

Baseline Launch Trajectory

For this study, a typical or baseline launch trajectory is similar to that presented in a study by Lepsch.[1] The trajectory, which is shown in Fig. 1, was divided into two segments:

1) *Initial climb and acceleration.* Initially powered by liquid hydrogen turbine and ramjet engines, the hypersonic vehicle climbs to

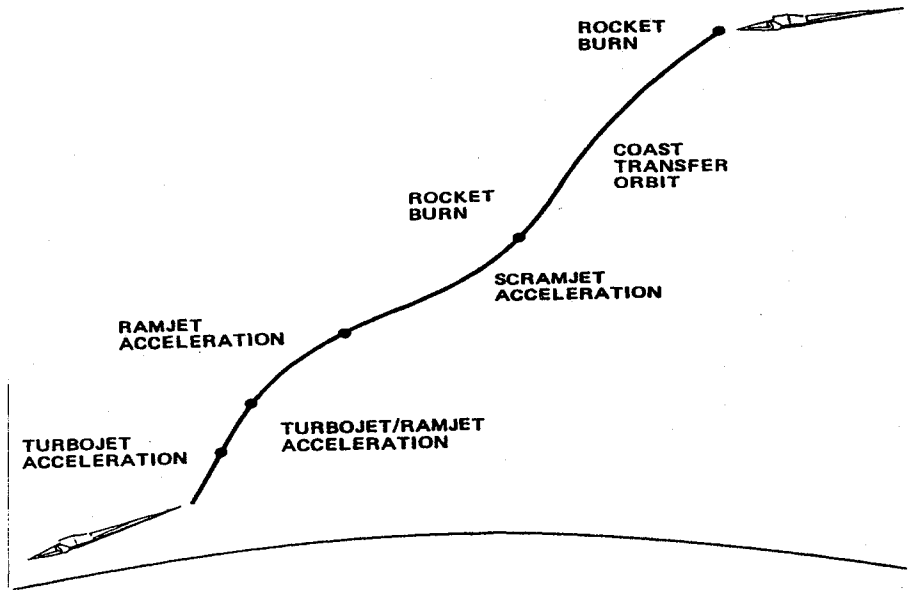

Fig. 1 Baseline ascent profile.

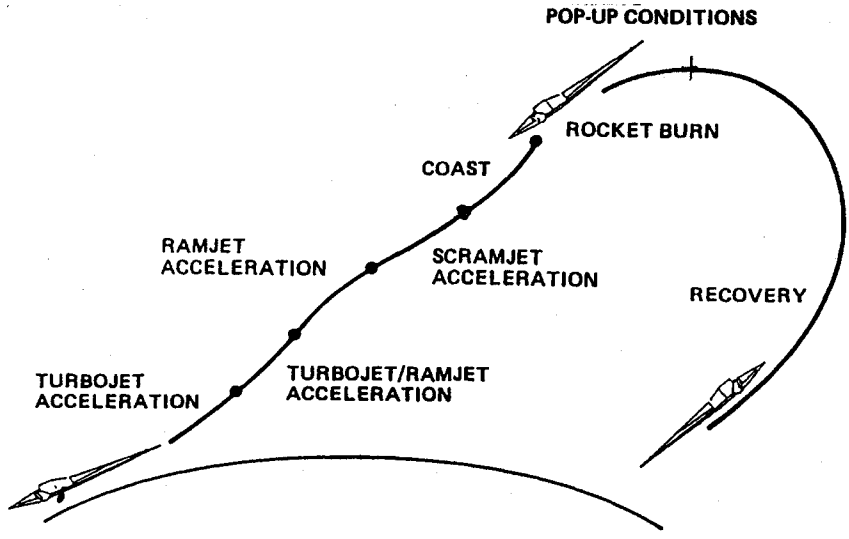

Fig. 2 Suborbital ascent profile.

an altitude of approximately 21,340 m and a speed of about Mach 6. Then, using supersonic combustion ramjet (scramjet) engines, the vehicle accelerates to a speed of about Mach 20 while gradually increasing altitude to about 51,800 m (the final speed desired to be attained at the end of this phase is subject to debate, with values in current literature ranging from Mach 8 to Mach 22).

2) *Orbit insertion.* Having accelerated as far as practical using air-breathing propulsion systems, a transition is made to rocket propulsion, which provides the additional thrust required to insert the launch vehicle into a low earth orbit. The velocity at which transition occurs is called the transition velocity.

Suborbital Launch Trajectory

The suborbital launch trajectory analyzed is depicted in Fig. 2. This trajectory can be divided into three segments. The first is similar to that of the baseline trajectory except that the transition velocity may be reduced from that of a baseline launch. The main difference from the baseline trajectory is introduced in the second segment, where rocket propulsion is used to raise the launch vehicle to higher altitudes without accelerating the vehicle to orbital velocity. For the third segment, the payload is separated from the launch vehicle shortly before the flight-path apogee and is inserted into the desired orbit by a small rocket booster. After payload separation, the launch platform falls back into the atmosphere and returns to a landing site. Note that the focus was on the ascent portion of suborbital trajectories and no effort was made to analyze the return-to-base portion of the launch-vehicle flight path.

Computational Methods

A traditional and complete investigation of launch ascent trajectory performance requires the use of complex numerical methods that incorporate various Earth, aerodynamic, and launch-vehicle modeling techniques. For this study, a simplified energy analysis method was developed, which provides a first-order approximation of suborbital launch trajectory performance. A more detailed analysis was also performed using a commercially available program named Optimal Trajectories by Implicit Simulations, or OTIS.[2] Results of the two methods were compared to identify differences between the analytical techniques.

For this investigation, conditions were imposed for both the energy analysis and OTIS trajectory optimization methods to assure that results obtained could be compared on an equal basis: 1) one launch-vehicle design was used for both the baseline and suborbital trajectories, and it was assumed that the gross takeoff weight for the launch vehicle was the same regardless of which trajectory was to be flown; 2) any propellant saved by flying along a suborbital

trajectory rather than the baseline trajectory was assumed to be additional payload capacity (payload + booster); 3) the payload of both the baseline and suborbital trajectories was delivered to a circular orbit 185.2 km (100 n mile) above the earth surface; and 4) a spherical nonrotating Earth was assumed.

A representative vehicle design similar to one used by Drummond[3] was used for this study. However, various design values for the vehicle shown in Fig. 3 were scaled up so as to represent an advanced hypersonic lifting body with lightweight structures and propulsion as discussed by Kasten.[4]

When considering various launch ascent profiles, there are an infinite number of individual trajectories that could be analyzed. In order to limit the trajectories studied, thermal and dynamic-pressure flight constraints were applied so that ascent profiles would be representative of the vehicle design presented in Fig. 3. First, dynamic-pressure limits were applied as follows: 1) a minimum dynamic pressure limit of 100 psf for the air-breathing ramjet–scramjet portion of flight, which was representative of the inlet pressure that would be required for proper engine performance, and 2) a maximum dynamic pressure of 0.5 psf at the deployment point, which was representative of conditions that would be required for this type of satellite deployment. Implementation of these dynamic-pressure limits allowed the altitude of the transition and deployment points to be calculated as a function of the velocity at these locations.

An exponentially distributed atmosphere as shown in Eq. (1) combined with the dynamic pressure relationship in Eq. (2) produced a formula for calculating an altitude based on velocity and dynamic pressure as shown in Eq. (3), where q is the dynamic pressure at the transition point:

$$\rho = \rho_0 e^{-H/Z} \tag{1}$$

$$q = (\rho V^2/2) \tag{2}$$

$$H = -Z\,\ell n(2q/\rho_0 V^2) \tag{3}$$

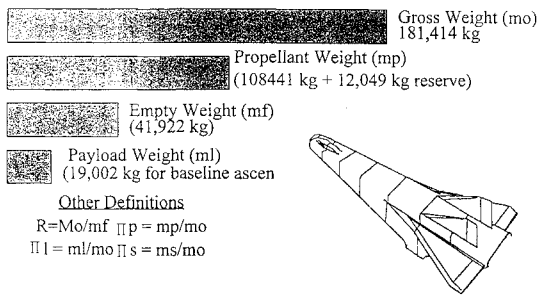

Fig. 3 Representative vehicle design weights.

Thermal constraints were applied in the form of maximum allowed normal shock temperature for the air-breathing portion of flight. For this study, a maximum normal shock temperature of 6500 K was applied consistent with an advanced vehicle design. Data for normal shock temperature based on velocity and altitude was obtained from a study by Huber as shown in Fig. 4.[5] This data was used to determine maximum velocity limitations associated with the air-breathing portion of flight and thereby identify the transition-point velocity.

Energy Analysis Method

The energy analysis method developed for this study was used to investigate the difference in performance of the two ascent trajectories defined above. First, the performance of the baseline trajectory for which both the launch vehicle and payload were placed in orbit was determined. Next, similar calculations were performed for the same launch vehicle flying a suborbital trajectory where only the payload is placed in orbit and the launch vehicle itself does not achieve orbital velocity but re-enters the atmosphere and returns to base.

The basis for the energy analysis formulated for this investigation consisted of mass-fraction definitions as given in Fig. 3 and the relationships shown below[6]:

$$V_{\text{cir}} = \sqrt{\mu/r_{\text{cir}}} \tag{4}$$

$$\xi = (V^2/2) - (\mu/r) \tag{5}$$

$$\Delta V = I_{\text{sp}} g_o \ell n R \tag{6}$$

$$R = e^{\Delta V/I_{\text{sp}} g_o} \tag{7}$$

Note that Eq. (7) was derived from Eq. (6), resulting in an approximation for the launch trajectory in that drag forces were not directly allowed for. Only a single I_{sp} value was used in Eq. (7) to represent the performance over a large segment of flight. For this reason, an average effective specific impulse was used in conjunction with Eq. (7) that would be representative of engine performance over the range of air-breathing flight. This average $I_{\text{sp eff}}$ is representative of air-breathing engine performance and will vary with velocity according to the thrust and air drag at various velocities as follows:

$$I_{\text{sp eff}} = (\text{thrust} - \text{drag})/\dot{m} \tag{8}$$

Values for $I_{\text{sp eff}}$ were generated from absolute I_{sp} data as shown by data points in Fig. 5. An average value of $I_{\text{sp eff}}$ was obtained by taking an average of $I_{\text{sp eff}}$ data points over the desired range

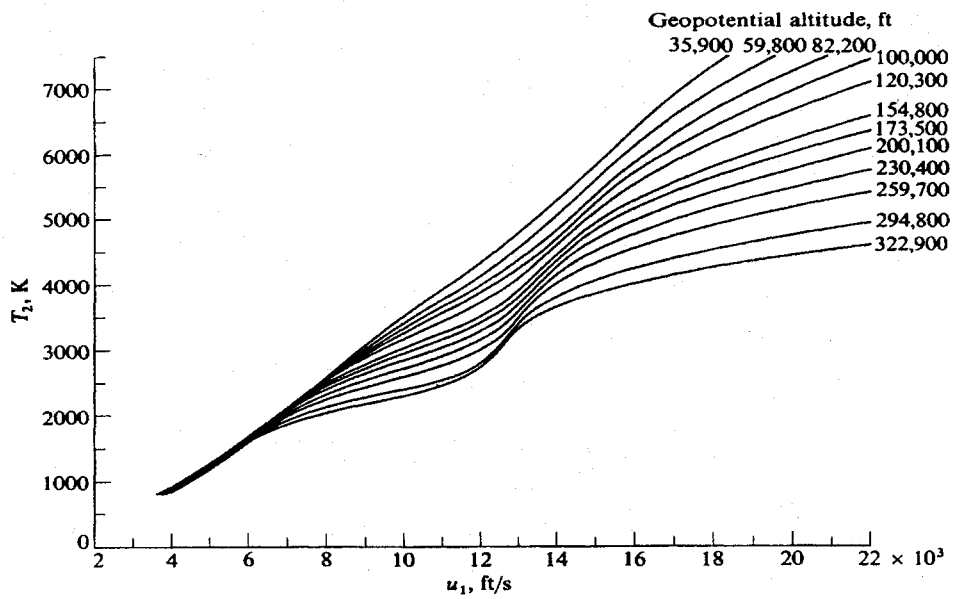

Fig. 4 Variation of normal shock temperature with velocity and altitude.[5]

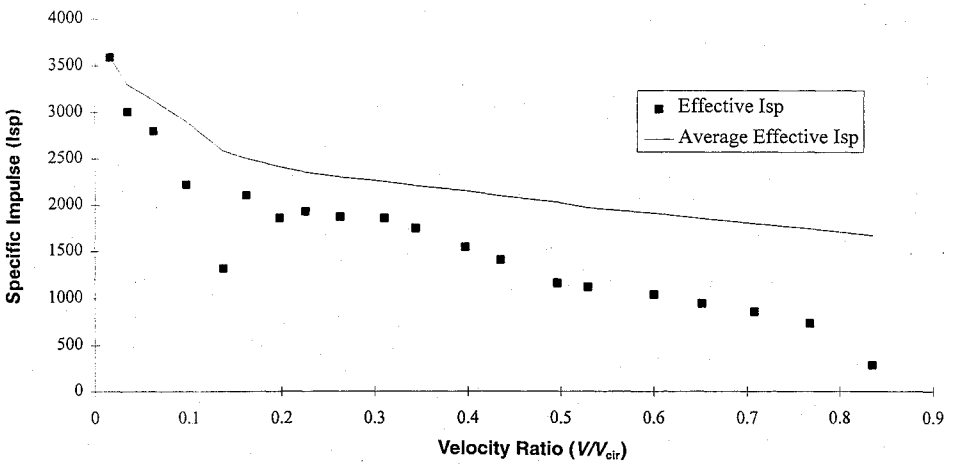

Fig. 5 Average specific impulse vs vehicle velocity.

of flight velocities. Average $I_{sp\ eff}$ data are shown as a solid line in Fig. 5. They vary with vehicle velocity because any given I_{sp} value represents an average from zero velocity to the appropriate Mach number at the end of the air-breathing portion of the ascent.

Baseline Vehicle Performance

The first step in the energy analysis method was to identify a baseline trajectory and determine its payload capacity. Since there were an infinite number of different ascent trajectories that could be identified, each with different performance characteristics, it was important to identify an ascent profile that would maximize the payload capacity of the baseline trajectory. For this study, the determination of an optimized trajectory involved identifying the velocity and altitude of the baseline transition point associated with the maximum-performance ascent trajectory. In this case, the optimum baseline trajectory would be achieved by maximizing the use of air-breathing propulsion, because the fuel specific-impulse performance of air-breathing engines is better than that of rocket engines. With this concept in mind, an iterative approach was used with thermal data from Fig. 4 and dynamic-pressure limits from Eq. (3) to determine the maximized transition-point altitude and velocity.

Once a particular baseline trajectory was identified, the total ΔV required to move between different points along the trajectory was determined. By assuming an instantaneous propellant burn for each segment and that the total specific energy ξ, immediately following engine operation, remains constant for the segment, Eq. (5) was used to establish the relationship shown in Eq. (9). This relationship was rearranged as shown in Eq. (10) to determine the ΔV requirement for both the air-breathing and rocket propulsion segments of the baseline ascent trajectory:

$$\frac{(V_1 + \Delta V)^2}{2} - \frac{\mu}{r_1} = \frac{V_2^2}{2} - \frac{\mu}{r_2} \tag{9}$$

$$\Delta V = \sqrt{2\left(\frac{V_2^2}{2} - \frac{\mu}{r_2} + \frac{\mu}{r_1}\right)} - V_1 \tag{10}$$

Next, the amount of propellant consumed along the air-breathing and rocket-powered portions of the trajectory was estimated. This was done by calculating the vehicle mass ratio at the transition point and after orbit insertion using Eq. (7). An appropriate average effective I_{sp}, based on the transition velocity, was taken from Fig. 5 for the air-breathing portion, and an I_{sp} of 400 s (conservative representation of a LH_2- and LOX-powered rocket engine) was used for the rocket-powered portion of the ascent.

After calculating the vehicle mass ratios for the air-breathing and rocket-propelled segments, the amount of propellant consumed along each segment was determined using Eq. (11). The payload capacity of the baseline ascent trajectory was then determined from Eq. (12):

$$m_p = m_0 - m_0[1 - (1/R)] \tag{11}$$

$$m_l = m_0 - m_s - m_{p1} - m_{p2} \tag{12}$$

Suborbital Trajectory Analysis

For this portion of the analysis, performance for a wide variety of suborbital trajectories was calculated with transition-point velocities ranging from zero to orbital velocity. Note that to limit the number of possible suborbital trajectory variables, the same velocity was used for both the transition and deployment points. In other words, the rocket-powered portion of flight in segment 2 of suborbital trajectories was used to increase the vehicle altitude while maintaining constant vehicle speed.

The first step in this analysis required the calculation of transition and deployment altitudes using Eq. (3). Once these altitudes were determined, the suborbital trajectory analysis was performed in a manner similar to that used with the baseline trajectory calculations. First, the total ΔV required to move through each segment of the suborbital trajectory was approximated using Eq. (10). Next, the vehicle mass ratio was calculated for the transition and deployment points using Eq. (7). As was done with the baseline trajectory analysis, an appropriate average effective I_{sp} value from Fig. 5 was used in Eq. (7) to determine the air-breathing mass ratio.

Next, the amount of propellant consumed prior to payload deployment was determined. To do this, the definition for the mass ratio R was manipulated to the form

$$m_p = m_0 - m_0[1 - (1/R)] \tag{13}$$

which was used once to calculate the propellant used during the air-breathing portion of flight and again for the rocket-powered portion of flight leading up to payload deployment. The total propellant consumed in the first two flight segments represented the total launch-vehicle propellant requirement for a particular suborbital trajectory. The difference between this sum and the propellant consumed by the baseline vehicle (i.e., baseline-vehicle propellant minus suborbital-vehicle propellant) was assumed to represent additional payload capacity for the combination of booster–kickmotor and payload m_{0so}. The initial weight of this combination was found by subtracting the weight of propellant consumed and the launch-vehicle structural weight from the initial launch-vehicle gross weight:

$$m_{0so} = m_0 - m_s - m_{p1} - m_{p2} \tag{14}$$

The payload weight placed in orbit by the booster motor was determined by calculating the ΔV requirement from deployment to orbit insertion using Eq. (10). For this calculation, the booster mass ratio R_{so} was calculated using Eq. (7). Assuming a conservative

value of 0.1 for booster–kickmotor structural mass ratio $\Pi_{s\,so}$, the payload weight delivered to orbit was then found using

$$m_l = (m_{0\,so}/R_{so}) - \Pi_{s\,so} m_{0\,so} \tag{15}$$

Finally, the vehicle performance for the suborbital trajectory was compared with that of the baseline vehicle using a payload ratio defined by

$$\text{payload ratio} = m_{l_{so}}/m_{l\,\text{baseline}} \tag{16}$$

A payload ratio greater than 1.0 indicated that the particular suborbital trajectory was capable of delivering a heavier payload to the target orbit than was possible with the baseline trajectory.

OTIS Analysis Method

To perform a comparison and validation of the energy analysis results, a more complex baseline and suborbital trajectory optimization was performed using the OTIS trajectory optimization program. OTIS uses several advanced numerical methods along with Earth, atmospheric, and vehicle models to facilitate the development of optimized flight paths. This program provides a high-fidelity representation of launch-vehicle performance based on the trajectory and flight-path constraints identified by the analyst.

For this study, OTIS was used to optimize a baseline and several suborbital trajectories as described for the energy analysis method. The same constraints and representative vehicle design were used for this analysis as were previously discussed with the energy analysis. In addition, aerodynamic characteristics were required to model subsonic and transonic flight regimes for each trajectory.

The OTIS analysis consisted of three phases:

1) The various models and flight constraints that would be used for the analysis were described. This included models for the launch vehicle, propulsion systems, aerodynamic performance, and atmospheric conditions. Constraints were included for engine inlet dynamic pressure, maximum heat flux, maximum acceleration, and allowable engine settings.

2) Next, the program was used to identify an optimized baseline trajectory and a series of several different suborbital trajectories based on the vehicle model and flight-path constraints.

3) Finally, the suborbital trajectory performance was compared with that of the baseline trajectory, using Eq. (16) as in the energy analysis.

The reader can find a more detailed discussion of the OTIS analysis in Refs. 2 and 7.

Results

The first area analyzed was the baseline trajectory. Although there are many different baseline transition point velocities and altitudes that could be analyzed, it was important to select conditions that would maximize the payload capacity of the baseline trajectory. Inspection of the vehicle design parameters and constraints applied for this study made it possible to identify an optimized baseline ascent profile. Since the air-breathing engine was more efficient than rocket propulsion, the highest performance was obtained by maximizing this segment of flight. Application of the dynamic-pressure and thermal constraints bound the baseline trajectory to a transition velocity of 6827 m/s (Mach 20.7) and an altitude of 44,622 m.

Once the optimized baseline transition point was identified, the propellant requirements and payload capacity were calculated. Based on the vehicle design and performance parameters previously discussed, the baseline propellant requirement was 108,441 kg. Subtracting the required propellant and structural weight from the gross weight resulted in 19,002 kg available as deliverable payload capacity.

After the baseline trajectory performance was determined, various suborbital trajectories were analyzed and the results compared with the baseline. A full range of suborbital trajectories was analyzed with transition-point velocities ranging from near zero to orbital velocity. For each individual trajectory, values were calculated for 1) launch-vehicle propellant requirement, 2) booster engine weight for orbit insertion, and 3) final payload weight. Suborbital trajectory results were then compared against the baseline trajectory by calculating payload ratio vs suborbital transition-point velocity as shown in Fig. 6. The following observations can be made from the results shown in Fig. 6:

1) The use of suborbital trajectories shows potential for increasing the payload-to-orbit capacity over that possible with a normal ascent profile as represented by the baseline trajectory. This observation is based on the portion of Fig. 6 where the payload ratio is greater than 1.0.

2) The best suborbital trajectory performance was achieved when the suborbital trajectory was initiated at a velocity slightly less than that of the baseline transition point. This observation has some intuitive support in that the best performance trajectory would be expected to take full advantage of the higher performance of the air-breathing engines prior to the transition point. At still higher transition-point velocities, the advantage of higher air-breathing engine performance is reduced as indicated by the I_{sp} values in Fig. 5.

3) Figure 6 shows a best-case suborbital payload capacity that is 50% greater than that of the baseline trajectory. The best-case suborbital trajectory resulted in a 28,617-kg payload capacity, as compared to the 19,002-kg payload capacity of the baseline trajectory.

4) From Fig. 6, it is apparent that an increase in payload placed in orbit can result from using suborbital launch trajectories with transition from air-breathing propulsion to rocket propulsion at a flight Mach number greater than approximately 13. Performance continues to increase, on a near-linear basis, until the suborbital transition velocity nears that of the baseline ascent profile.

The energy analysis suborbital trajectory results are compared with the suborbital trajectory performance calculated with OTIS in Fig. 7, where the energy analysis results are identified by a solid line and OTIS data by individual points. The following observations can be made based on the data shown in Fig. 7:

1) A very good correlation exists between the OTIS and energy analysis results. Note that the energy analysis results are conserva-

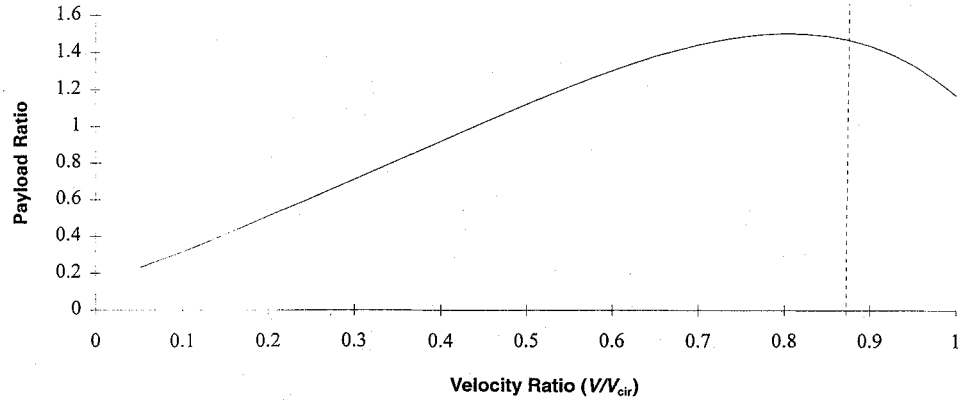

Fig. 6 Comparison of suborbital and baseline trajectory performance with various suborbital transition-point velocities.

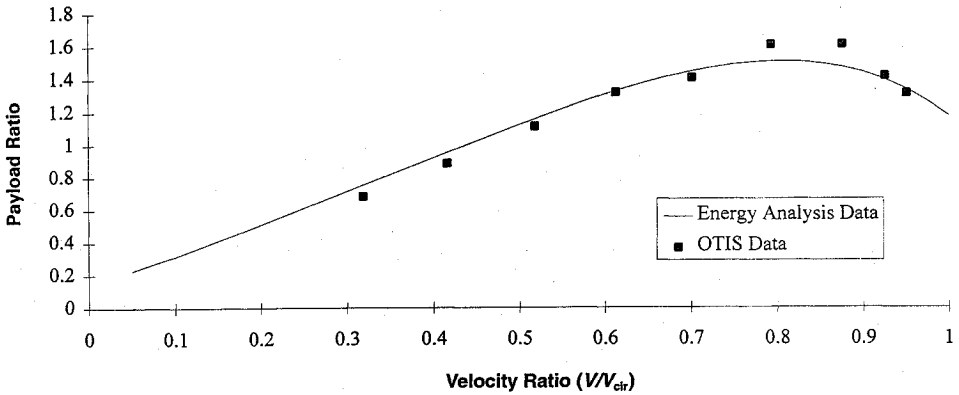

Fig. 7 Comparison of energy analysis and OTIS analysis results.

tive compared to the OTIS results for suborbital trajectories with transition velocities near the baseline transition point. Some variation between the two techniques might be expected as a result of the differences between the two methods used to calculate the results and the simplifying assumptions adopted for the energy analysis method.

2) The OTIS results indicated an even greater suborbital payload capacity than that obtained with the energy analysis. OTIS results indicate a best-case suborbital payload capacity that is 61% greater than that of the baseline trajectory, as compared to a 50% increase identified using the energy analysis.

Conclusions

The primary conclusion from this study involves the utility of the energy analysis method that was developed for the analysis of suborbital trajectories. Based on the results and on comparison with results from the more rigorous OTIS analysis, it appears that the energy analysis method provides an excellent tool for initial hypersonic-vehicle performance and design calculations. Results from this method can be obtained quickly and without much computer support. This method is also useful for exploring many different vehicle designs as part of an initial concept of employment for this type of vehicle.

Although the focus of this study was to investigate the utility of a simplified analysis tool, there are other conclusions from the results of this study as follows:

1) The use of suborbital trajectories shows potential for increasing the payload weight that can be placed in orbit from a hypersonic-lifting-body vehicle. Results from this study indicated up to 61% increase in payload capacity is possible over the conventional hypersonic-lifting-body trajectory in which both the launch vehicle and payload are placed in orbit.

2) Based on the vehicle design used for this study, the optimum point for transition from air-breathing propulsion to rocket propulsion appears to be at a speed ratio of approximately 0.876 (Mach 20.7) and an altitude ratio approximately 0.279 (44,622 m), regardless of whether a baseline or suborbital ascent is used. While the realization of a hypersonic vehicle that can achieve this level of performance promises to be a challenge, results from this analysis indicate that the largest payload ratios would result from this type of ascent profile.

References

[1]Lepsch, R. A., Jr., et al., "Utilizing Air–Turborocket and Rocket Propulsion Systems," AIAA Paper 90-0295, Jan. 1990.

[2]Martens, P. J., "Optimal Trajectories by Implicit Simulation, Applications Manual," Boeing Aerospace and Electronics, Dec. 1990.

[3]Drummond, A. M., "Performance and Stability of Hypervelocity Aircraft Flying on a Minor Circle," Univ. of Toronto Inst. for Aerospace Studies, UTIAS TR 135, Toronto, ON, Canada, Dec. 1968.

[4]Kasten, T. D., "A National Utility Review," Society of Automotive Engineers, Paper 91-1170, April 1991.

[5]Huber, P. W., "Hypersonic Shock-Heated Flow Parameters for Velocities to 46,000 Feet per Second and Altitudes to 323,000 Feet," NASA TR R-163, Dec. 1963.

[6]Sutton, G. P., *Rocket Propulsion Elements*, 6th ed., Wiley, 1992, Chap. 5.

[7]Goodell, M. R., "Analysis of Ballistic Launch Trajectories for Satellite Delivery," M.S. Thesis, Graduate School of Engineering, Air Force Inst. of Technology (AU), AFIT/GSO/ENS/91D-6, Wright-Patterson AFB, OH, Dec. 1991.

J. A. Martin
Associate Editor